www.nature.com/aps

Acta Pharmacologica Sinica

ARTICLE

Chitosan oligosaccharide modified liposomes enhance lung cancer delivery of paclitaxel

Yun-qiu Miao[1,2], Ming-shu Chen[1,2], Xin Zhou[2], Lin-miao Guo[2,3], Jing-jing Zhu[2], Rui Wang[1], Xin-xin Zhang[2,3] and Yong Gan[2,3]

Lung cancer is one of the leading causes of cancer-related death worldwide. Various therapeutic failed in the effective treatment of the lung cancer due to their limited accumulation and exposure in tumors. In order to promote the chemotherapeutics delivery to lung tumor, we introduced chitosan oligosaccharide (CSO) modification on the liposomes. CSO conjugated Pluronic P123 polymers with different CSO grafting amounts, called as CP50 and CP20, were synthesized and used to prepare CSO modified liposomes (CP50-LSs and CP20-LSs). CP50-LSs and CP20-LSs displayed significantly enhanced cellular uptake in A549 cells in vitro as well as superior tumor accumulation in vivo compared with non-CSO modified liposomes (P-LSs). This phenomenon was related to the increased affinity between CSO modified liposomes and tumor cells following massive adsorption of collagen, which was highly expressed in lung tumors. In the A549 tumor-bearing mouse model, intravenous injection of paclitaxel (PTX)-loaded CP50-LSs every 3 days for 21 days resulted in optimal antitumor therapeutic performance with an inhibition rate of 86.4%. These results reveal that CSO modification provides promising applicability for nanomedicine design in the lung cancer treatment.

Keywords: lung cancer; antitumor; chitosan oligosaccharide; liposomes; paclitaxel; drug delivery; nanomedicine

Acta Pharmacologica Sinica (2021) 42:1714–1722; https://doi.org/10.1038/s41401-020-00594-0

INTRODUCTION

Lung cancer has the highest mortality among all cancers worldwide [1]. The 5-year survival rate of nonsmall cell lung cancer patients remains below 20%, and this high rate of mortality has been maintained over the years [2]. Current clinical therapies, including small molecule chemotherapeutics and macromolecular antibodies, still face the difficulty of insufficient exposure to tumors, limiting their therapeutic efficacy in lung cancer [3, 4]. More recently, nanomedicine has become an alternative and emerging option as a therapeutic agent for cancer therapy. For example, large nanoparticles are designed to accumulate in the lungs due to the biological interception of pulmonary capillaries [5, 6]. Advanced strategies that functionalize nanoparticle surfaces with ligands have been reported to bind to receptors overexpressed on tumor cells and produce targeted effects in lung cancer treatment [7]. However, in practice, larger nanoparticles are prone to pulmonary embolism after intravenous injection, causing severe side effects and even breathing difficulties in patients [8]. Few targeting strategies translate into clinical success due to difficulties in achieving cell-specific targeting of nanoparticles in vivo [9]. Therefore, nanomedicine delivery to lung tumors is challenging.

Biodegradable polymers have been extensively investigated for drug delivery, such as poly(lactic-co-glycolic) acid [10, 11], polyethylenimine [12, 13], and chitosan [14, 15]. Among them, chitosan is recognized as a nontoxic, biocompatible, and biodegradable polymer [16–18] and has been widely exploited for biomedical and pharmaceutical applications [19, 20]. Notably, chitosan has been reported to show strong adhesion with lung cancer cells due to its positive charge and mucoadhesive property [21, 22], thus promoting nanocarrier internalization [23]. However, the use of high-molecular-weight chitosan has certain drawbacks because of its low solubility at physiological pH, its high viscosity [24] and the fact that the chitosan complexes often tend to form aggregates [25]. It is necessary to design nanocarriers with novel biomaterials for drug delivery and treatment of lung cancers.

In this study, chitosan oligosaccharide (CSO) was conjugated with Pluronic P123 polymer to synthesize the new biomaterials CP50 and CP20 and modified on liposomes to improve drug delivery to lung tumors. CSO is the chemical or enzymatic depolymerization product of chitosan [26]. The low molecular weight and water solubility of CSO can overcome the limitations of chitosan as a drug carrier, and it has been proven to be an effective vector for drug delivery [27, 28]. Pluronic P123, as an amphiphilic block copolymer, can endow liposomes with steric stabilization and increase the solubility of hydrophobic drugs. CP50- and CP20-modified liposomes (CP50-LSs and CP20-LSs) are expected to show enhanced affinity for lung tumor cells and to increase the accumulation of liposomes in lung tumors. Paclitaxel (PTX), which has been widely used in the treatment of nonsmall cell lung cancer in clinical trials [29, 30], was used as a model drug to be encapsulated into CP50-LSs and CP20-LSs to study the potential therapeutic effect in A549 nonsmall cell lung cancer models.

MATERIALS AND METHODS

Pluronic P123 (PEO_{20}-PPO_{70}-PEO_{20}) and the near-infrared fluorescent dye IR783 were obtained from Sigma Aldrich (St Louis, MO, USA). CSO (1162 kDa, deacetylation degree: >90%) was obtained from

[1]School of Pharmacy, Shanghai University of Traditional Chinese Medicine, Shanghai 201203, China; [2]Shanghai Institute of Materia Medica, Chinese Academy of Sciences, Shanghai 201203, China and [3]University of Chinese Academy of Sciences, Beijing 100049, China
Correspondence: Rui Wang (ellewang@163.com) or Xin-xin Zhang (xinxinzhang@simm.ac.cn) or Yong Gan (ygan@simm.ac.cn)

Received: 3 September 2020 Accepted: 1 December 2020
Published online: 19 January 2021

Shandong Weikang Biomedical Technology Co., Ltd. (Linyi, China). *N*, *N'*-Disuccinimidyl carbonate (DSC), 4-dimethylaminopyridine (DMAP), coumarin 6, acetonitrile, ether, ethanol and cholesterol were obtained from Sinopharm Chemical Reagent Co., Ltd. (Shanghai, China). PTX (98%), DAPI, Hoechst 33342, 3-(4,5-dimethylthiazol-2-yl)-2,5-diphenyltetrazolium bromide (MTT), Dulbecco's modified Eagle's medium (DMEM), penicillin-streptomycin, 0.25% trypsin EDTA solution and collagen type I were purchased from Dalian Meilun Biotechnology Co., Ltd. (Dalian, China). Fetal bovine serum (FBS) was purchased from Life Technologies Corp. (Grand Island, NY, USA). Alexa Fluor 555-conjugated WGA was obtained from Invitrogen (Carlsbad, CA, USA). Egg yolk lecithin (PC-98T) was provided by Q.P. Corporation (Tokyo, Japan).

Cell line and cell culture

The human nonsmall cell lung cancer cell line A549 was obtained from the Shanghai Institutes for Biological Sciences. The cells were cultured in DMEM with 10% FBS and 1% penicillin-streptomycin and maintained at 37% in a humidified atmosphere with 5% CO_2.

Animals

Male BALB/c *nu/nu* mice (4–6 weeks old, 20 ± 2 g) were obtained from the Animal Facility of the Shanghai Institute of Materia Medica (Shanghai, China). All animal experiments were reviewed and approved by the Institutional Animal Care and Use Committee of Shanghai Institute of Materia Medica, Chinese Academy of Sciences, Shanghai, China.

Synthesis of CSO-conjugated Pluronic P123 polymer

CSO-conjugated Pluronic P123 polymers were synthesized through a two-step process. First, Pluronic P123 (1.45 g, 0.25 mmol) was dissolved in acetonitrile (5–10 mL) and reacted with DSC (76.8 mg, 0.3 mmol) and DMAP (152.5 mg, 1.25 mmol) overnight to synthesize P123-SC. The product was precipitated with ether and dried in a vacuum. CP20 and CP50 were prepared by adding CSO to P123-SC solution, with CSO to Pluronic P123 molar ratios of 1:3 and 3:1, respectively. The resulting solution was stirred and allowed to react for 24 h. The product was dialyzed in water using a dialysis tube (molecular weight cutoff 3500 Da) to remove traces of unreacted CSO, evaporated and freeze-dried. The final product was stored at −20 °C until use. The molecular structure of the graft polymer was confirmed by Fourier transform infrared spectroscopy (Nicolet iS5 FT-IR, Thermo Fisher, USA). The CSO contents of CP20 and CP50 were determined by high-performance liquid chromatography (HPLC) with a mobile phase of phosphate buffer and acetonitrile (95/5, *v/v*) at a flow rate of 1.0 mL/min.

Preparation of PTX-loaded liposomes

CSO-modified liposomes were prepared by a thin-film hydration method. Briefly, CP20 or CP50 (15 μmol), PC-98T (16.3 mg) and cholesterol (1.6 mg) were dissolved in ethanol (15 mL) and then dried to a thin lipid film. The dried lipid films were subsequently hydrated with PBS (pH = 7.4, 15 mL) at 45 °C to obtain liposome suspensions. The suspensions were finally extruded through a 100-nm polycarbonate membrane using a microextruder to obtain the CP20-LSs and CP50-LSs. For non-CSO-modified liposomes (P-LSs), Pluronic P123 (15 μmol) was dissolved in ethanol, desiccated, and then hydrated as described above.

For paclitaxel-loaded liposomes, polymers (CP20, CP50 or Pluronic P123, 15 μmol), PC-98T (16.3 mg), cholesterol (1.6 mg), and PTX (12 mg) were dissolved in ethanol, and all other materials and procedures were the same as described in the preparation of CSO-modified liposomes.

Characterization of liposomes

The particle size distribution and zeta potential of liposomes were determined by a Malvern Zetasizer Nano ZS analyzer (Worcestershire, UK). Liposomes were evaluated for morphology by transmission electron microscopy (TEM, Talos Arctica, Thermo, USA). To evaluate the safety of liposomes, A549 cells were seeded in 96-well plates at 10,000 cells per well. Blank liposomes (P-LSs, CP20-LSs, and CP50-LSs) at different concentrations were incubated with cells for 48 h. A MTT kit was used to assess cell viability. The stability of liposomes under physiological conditions was evaluated by suspending liposomes in pH 7.4 PBS containing 10% fetal bovine serum at 4 °C and recording the changes in the size of liposomes by dynamic light scattering.

PTX-loading efficiency (LE%) was determined by HPLC. In brief, an equal volume of methanol was added to PTX-loaded liposomes, followed by sonication and dilution with the mobile phase. The PTX loaded in the liposomes was analyzed by HPLC under the following chromatographic conditions: column, Agilent Zorbax SB-C18 (150 mm × 4.6 mm, 5 μm); column temperature, 30 °C; mobile phase, acetonitrile-water (53:47, v/v); detection wavelength, 227 nm; flow rate, 1.0 mL/min; and injection amount, 20 μL. PTX-loading efficiency was calculated using the following equation:

$$\mathrm{LE}\% = \frac{\text{Amount of PTX loaded in the liposomes}}{\text{Total amount of PTX} - \text{loaded liposomes}} \times 100\%$$

The in vitro release behavior of PTX from liposomes was measured using a dialysis method. One milliliter of PTX@P-LSs, PTX@CP20-LSs, and PTX@CP50-LSs were placed separately into a dialysis tube with a molecular weight cutoff of 8000–14,000 Da (Sinopharm Chemical Reagent, Shanghai, China) and dialyzed in 40 mL of PBS (pH 7.4 or pH 5.0) containing 0.2% Tween-80. At various times (0.5, 1, 2, 4, 8, 12, and 24 h), 1 mL of sample was replaced with an equal volume of fresh dialysis buffer, and the concentration of PTX in the sample was analyzed using HPLC.

Cellular uptake and antitumor efficacy of PTX-loaded liposomes

To evaluate the uptake efficiency into tumor cells, coumarin 6-labeled liposomes were incubated with A549 tumor cells seeded in a 12-well plate for 1 h. After the indicated incubation time, adherent cells were detached from the 12-well plate with 0.25% trypsin and collected for flow cytometry analysis using a BD Biosciences FACSCalibur flow cytometer (USA). The analysis was performed using FlowJo software. For imaging, the cells were cultured on a glass coverslip followed by incubation with coumarin 6-labeled liposomes. After washing, the cell nucleus was stained with Hoechst 33342, and the cell membrane was labeled with Alexa 555-WGA and imaged by an Olympus FV1000 confocal laser scanning microscope (Japan).

For MTT analysis, A549 cells were seeded in 96-well plates at 10,000 cells per well. After 24 h of culture, A549 cells were incubated with PTX@P-LSs, PTX@CP20-LSs, and PTX@CP50-LSs at different concentrations for 48 h. Then, MTT measurement was performed, and the absorbance was detected at a wavelength of 490 nm.

Tumor accumulation of liposomes in vivo

A549 cells (5×10^6 cells) were subcutaneously implanted into the armpits of BALB/c *nu/nu* mice to establish xenograft tumor models. To evaluate the tumor accumulation of liposomes in vivo, NIRF imaging was performed with liposomes labeled with the near-infrared dye IR783. The A549 tumor-bearing mice were intravenously injected with fluorescence-labeled liposomes and imaged by the IVIS Spectrum System (Caliper Corp, Waltham, Massachusetts, USA) at 1 h and 6 h postinjection. After 6 h of injection, the main organs and tumors were collected for imaging, followed by quantitative analysis with a region of interest tool.

When the tumor volume increased to 200 mm^3, coumarin 6-labeled liposomes were injected intravenously. After 24 h, the tumor was removed for cryosection, stained with DAPI, and observed by confocal microscopy.

Identification of liposome-adsorbing proteins

The lung proteins in the interstitial fluid and cell membrane were collected as previously reported [31]. In brief, fresh lung tissue was cut into small pieces in PBS containing protease inhibitor cocktail on ice, washed carefully with PBS to remove the broken cells and intracellular proteins, and then incubated with fresh PBS at 37 °C for 1 h. After incubation, the sample was centrifuged at $1000 \times g$ for 3 min to remove the tissue pieces, and the supernatant was further centrifuged at $2000 \times g$ for 8 min to remove the cells. Finally, after centrifugation at $20{,}000 \times g$ for 30 min to remove other insoluble substances, such as cell debris, the supernatant was collected and snap-frozen in liquid nitrogen, followed by storage at −80 °C.

To investigate the interaction between liposomes and extracellular proteins in the lung, the liposomes were incubated with extracellular proteins from the lung (total protein concentration of 23 mg/mL). At the end of incubation (37 °C, 1 h), the liposomes were washed three times by centrifugation at $100{,}000 \times g$ at 4 °C in PBS using an ultracentrifuge (Hitachi, Japan). The pellets were resuspended in PBS for size measurements and in RIPA lysis buffer for BCA protein assay and SDS-polyacrylamide gel electrophoresis (SDS-PAGE).

To measure the adsorption of collagen on the liposomes, the liposomes were incubated with collagen for 1 h at 37 °C. After incubation, the liposome-collagen complexes were centrifuged and assessed using the BCA protein assay.

Cellular uptake of liposomes in the presence and absence of collagen

To investigate the effect of collagen on the cellular uptake of liposomes, A549 cells were seeded in a 12-well plate at a density of 1×10^5 cells per well and incubated in fresh serum-free medium for 1 h before the addition of coumarin 6-labeled liposomes. The liposomes were first incubated with collagen as described above and separated from residual proteins by centrifugation. Liposomes without or with collagen were then resuspended in serum-free medium before the dispersions were added to the A549 cells. After an incubation time of 1 h, adherent cells were detached from the 12-well plate with 0.25% trypsin and collected for flow cytometry analysis using a BD Biosciences FACSCalibur flow cytometer. Analysis was performed using FlowJo software.

In vivo antitumor efficacy

To evaluate the antitumor effect of different PTX formulations in vivo, a tumor xenograft animal model was established by subcutaneous inoculation of an A549 cell suspension (5.0×10^6 cells in 100 μL of serum-free medium) into the armpits of male BALB/c *nu/nu* mice. The tumors were allowed to grow to ca. 100 mm^3. The mice were then randomly divided into five groups with eight mice in each group. Free PTX, PTX@P-LSs, PTX@CP20-LSs, and PTX@CP50-LSs or PBS were intravenously injected every three days at a PTX dose of 10 mg/kg. Tumor volume and body weight were monitored during the treatment. Tumor volume was calculated by the following formula: volume = (length × $width^2$)/2. On day 22 after treatment, the tumors were removed from the euthanized mice to calculate the tumor inhibition rate (TIR): TIR (%) = $(1- W_{PTX}/W_{PBS}) \times 100$ %, where W_{PTX} and W_{PBS} are the mean tumor weights of the PTX formulation groups and the PBS group, respectively. Moreover, the tumor tissues were sectioned and then stained with hematoxylin and eosin for histological analysis.

Statistical analysis

All the data are presented as the mean ± SD. Statistical analysis was performed by Student's *t* test or ANOVA.

RESULTS

Characterization of PTX-loaded liposomes

CSO-conjugated Pluronic P123 polymers were synthesized through a diimide-activated amidation chemical reaction. As shown in Fig. 1a, the characteristic peaks of both Pluronic P123 and CSO were observed in the FTIR spectra of CP20 and CP50, suggesting the successful synthesis of CSO-conjugated Pluronic P123 polymers. The peak at 1610 cm^{-1} was assigned to the amino group bending vibration of CSO, and the different intensities of the amino adsorption peak indicated the different CSO contents in CP20 and CP50. The CSO content of CP50 was 4.2-fold higher than that of CP20 as determined by HPLC (Fig. 1b). CP20 and CP50 were used to prepare liposomes, which were referred to as CP20-LSs and CP50-LSs. The hydrodynamic diameters of CP20-LSs and CP50-LSs were approximately equal (~75 nm) and similar to those of non-CSO-modified liposomes (P-LSs), and the morphology of the three liposomes was spherical with a clear membrane structure as observed by TEM (Fig. 1c, d). CSO-modified liposomes exhibited a higher surface charge than non-CSO-modified liposomes (P-LSs), which also reflected the existence of CSO. With CSO modification, the zeta potential of liposomes increased from −2 mV to 3 mV, being neutral (Fig. 1e). The nonpositively charged liposomes had no inhibitory effect on A549 cells, indicating high safety for drug delivery (Fig. 1f). The stability of P-LSs and CSO-modified liposomes was investigated in serum-containing media. All the liposomes showed little change in size over 1 week, suggesting their stability in biologically relevant media (Fig. 1g).

PTX, representing the most classical example of antitumor drugs, was loaded in liposomes, and the drug-loading efficiency of liposomes was ~10% (Fig. 1 h). Then, we evaluated drug release over a period of 24 h at different pH values. The cumulative release of PTX from PTX@P-LSs, PTX@CP20-LSs, and PTX@CP50-LSs at physiological pH after 24 h was 59.4%, 59.2% and 56.3%, respectively, indicating that PTX was steadily incorporated in the liposomes (Fig. 1i). After lowering the pH to 5.0, the cumulative PTX release from liposomes increased from 50% to 90% at 12 h, suggesting the rapid release of PTX from liposomes in the intracellular endosomal environment (Fig. 1j). This may be attributed to the destabilization of the lipid layer in the acidic environment. Overall, liposomes loaded with PTX were successfully fabricated with similar physical and chemical properties, leaving the CSO content of liposomes as the only variable factor.

Cellular uptake and antitumor efficacy of PTX-loaded liposomes

To investigate the effect of CSO modification on the cellular uptake of liposomes, A549 cells were incubated with coumarin 6-labeled liposomes, followed by observation with confocal microcopy and quantitative analysis using flow cytometry. P-LSs showed a weak fluorescence signal in A549 cells, owing to the steric hindrance of hydrophilic PEO chains, as previously reported [32]. Both CSO-modified liposomes exhibited enhanced cellular uptake compared with P-LSs. Notably, CP50-LSs showed higher fluorescence intensity in the cytoplasm, with a 1.9-fold higher signal intensity than CP20-LSs (Fig. 2a–c). Furthermore, a Z-stack scan of the whole cell layer was performed to evaluate the distribution of the three liposomes in cells. As shown in Fig. 2d, e, the signal of P-LSs was observed in a narrow area in the z direction with a thickness of ~4 μm, indicating the poor internalization of liposomes modified with PEO chains in tumor cells. In contrast, CP20-LSs and CP50-LSs distributed deeper in the cell layers than P-LSs, with depths of ~11 and ~14 μm, respectively. A large amount of CP50-LSs was distributed in the whole cytoplasm, suggesting that internalization of CP50-LSs was faster than that of CP20-LSs and P-LSs. Collectively, CP50-LSs with more CSO modifications on the surface of liposomes showed faster and more efficient cellular internalization than CP20-LSs and P-LSs.

Based on the cellular uptake in A549 cells, PTX@CP50-LSs were expected to exhibit superior antitumor efficacy in A549 tumor cells. Compared to PTX@P-LSs and PTX@CP20-LSs, PTX@CP50-LSs demonstrated higher cytotoxicity in a dose-dependent manner (Fig. 2f), which could be explained by the enhanced intracellular PTX concentration caused by the increased cellular uptake of CSO-

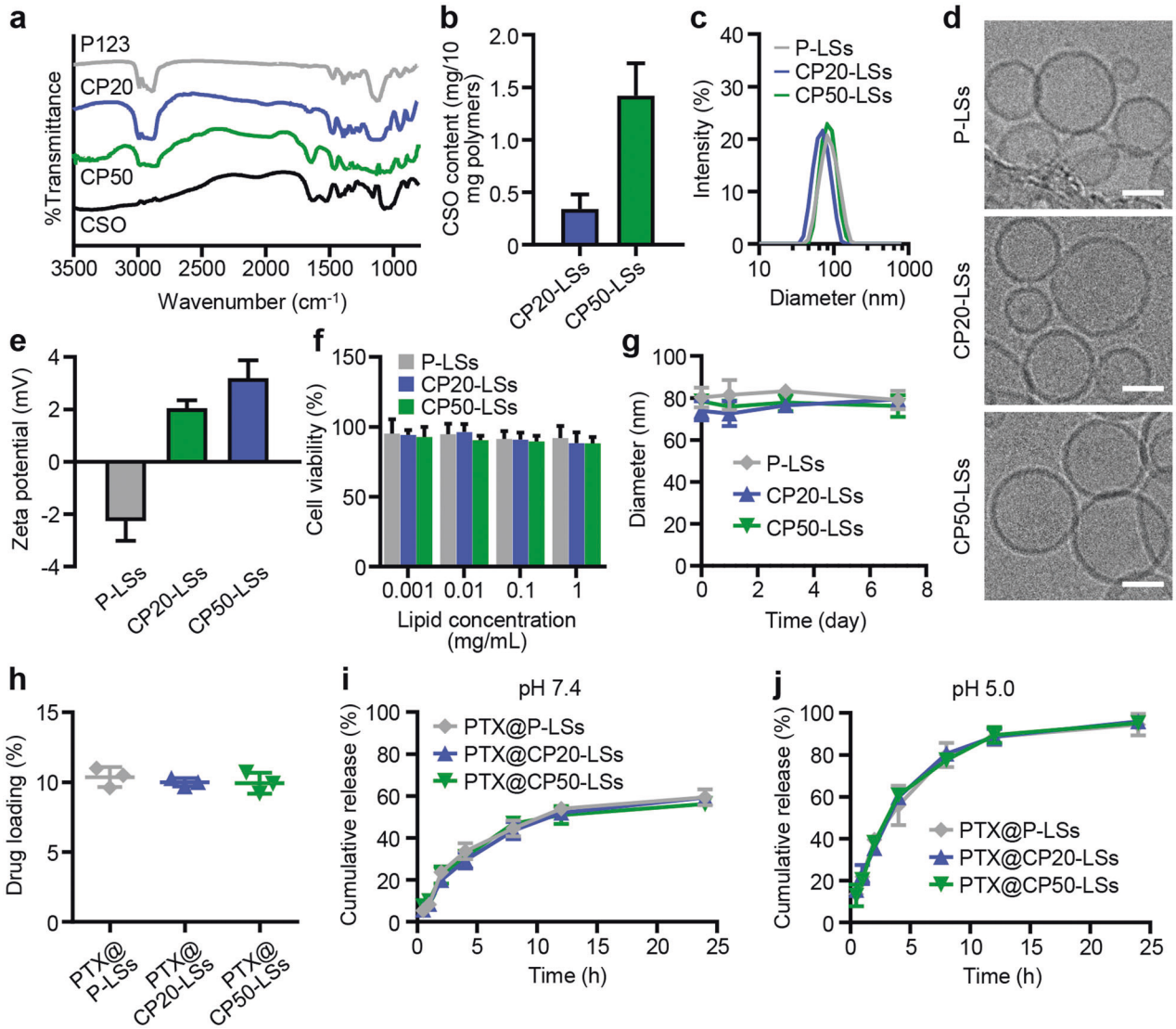

Fig. 1 Characterization of PTX-loaded liposomes. a FT-IR spectra of CP20 and CP50. **b** The CSO contents of CP20 and CP50 as determined by HPLC. **c** The size distribution of P-LSs, CP20-LSs, and CP50-LSs. **d** TEM images of P-LS, CP20-LSs and CP50-LSs. Scale bar = 50 nm. **e** The zeta potential of P-LSs, CP20-LSs, and CP50-LSs. **f** Cell viability of A549 cells incubated with blank liposomes of various concentrations. **g** The stability of P-LSs, CP20-LSs, and CP50-LSs in 10% serum-containing PBS, reflected by particle size over time. **h** Drug-loading efficiency of P-LSs, CP20-LSs and CP50-LSs. **i** The cumulative release of PTX from PTX@P-LSs, PTX@CP20-LSs, and PTX@CP50-LSs when exposed to simulated body fluid (pH 7.4) and to (**j**) endosome/lysosome environment (pH 5.0) at 37 °C. All data are presented as the mean ± SD ($n = 3$).

modified liposomes. The IC_{50} value of PTX@CP50-LSs was 3.2 times lower than that of PTX@CP20-LSs in the A549 cell model due to the enhanced cellular uptake caused by a large amount of CSO on CP50-LSs (Fig. 2g). In general, PTX@CP50-LSs showed enhanced cellular uptake in A549 cells, resulting in excellent antitumor activity in vitro.

Tumor accumulation of liposomes in vivo

To investigate the distribution of CP50-LSs in vivo, noninvasive NIRF imaging was performed using liposomes labeled with the near-infrared dye IR783. After the intravenous administration of liposomes, a near-infrared signal was observed in the animal body and gradually distributed to various organs and tumors over time (Fig. 3a). For a more accurate measurement, we collected organs and tumors for fluorescence intensity analysis. The signal intensity of CP50-LSs in tumors was 2.6 and 1.6 times higher than that of P-LSs and CP20-LSs, respectively, indicating the high accumulation of liposomes with enhanced CSO modification (Fig. 3b, d). In addition, CP50-LSs were more heavily distributed in normal lung tissues than P-LSs, which may be caused by the bioadhesion of CSO on the liposome surface (Fig. 3c). We preliminarily inferred that CP50-LSs with high CSO content on the surface may easily accumulate in lung tissue, especially in lung tumors.

Then, we studied the distribution of liposomes in tumor tissue sections at high magnification. A stronger fluorescence signal was observed in the tumor sections treated with CP50-LSs than in those treated with P-LSs and CP20-LSs. In addition, the green fluorescence of CP50-LSs was observed in the whole area by confocal microscopy, with the P-LSs and CP20-LSs confined to narrow spaces (Fig. 3e). This may be attributed to the high cellular uptake of CP50-LSs and decreased re-entry of liposomes into the bloodstream, leading to efficient tumor accumulation. Moreover, we observed that CP50-LSs exhibited uniform internalization in the tumor cells in the partially enlarged images (Fig. 3e). In contrast, P-LSs were mainly located in the extracellular space, as the green fluorescence of liposome aggregations was distributed far from the nucleus, showing the poor cellular uptake of liposomes with Pluronic P123 modification. These results indicated

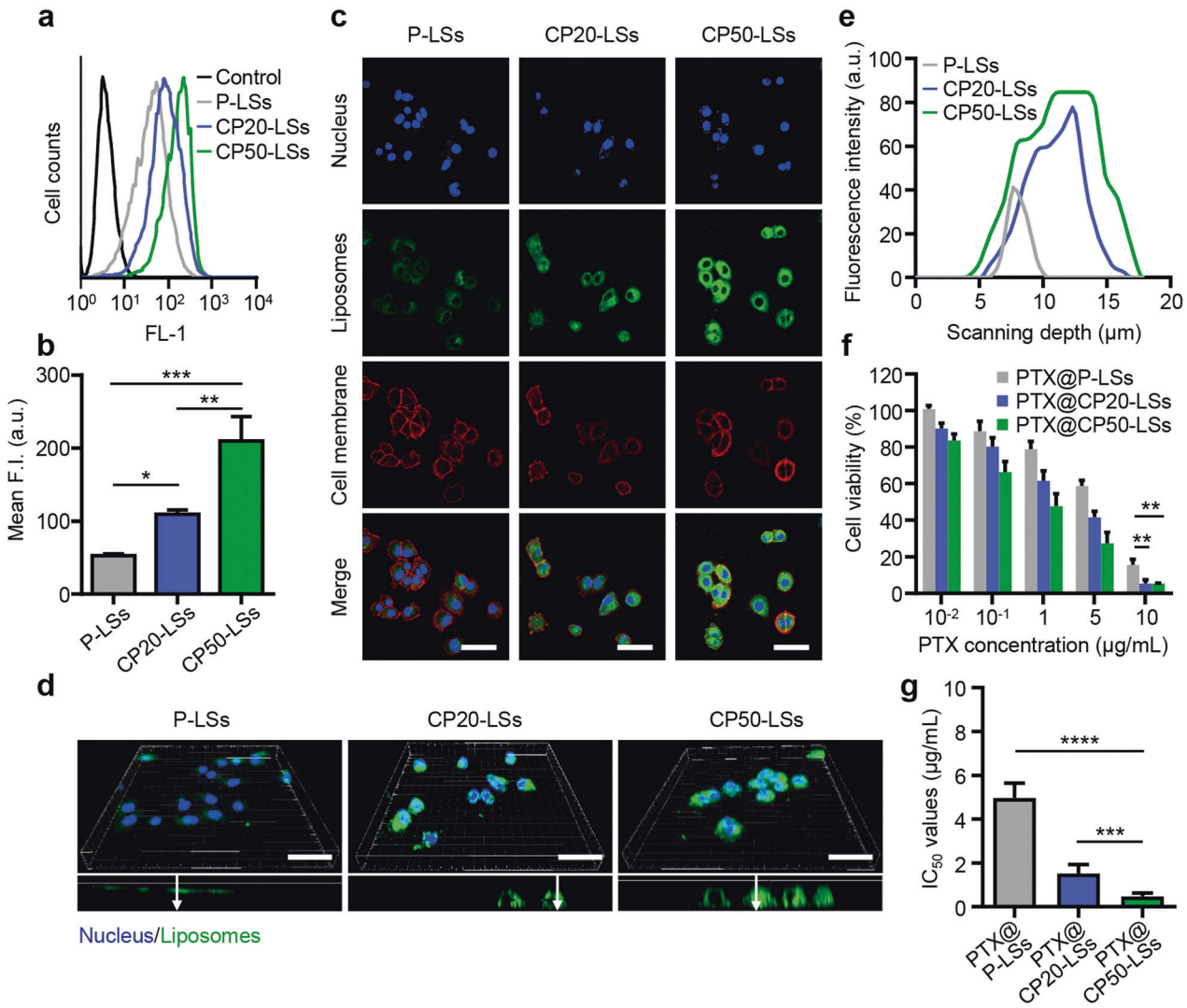

Fig. 2 Cellular uptake and in vitro antitumor efficacy of PTX-loaded liposomes. a Representative flow cytometry histograms of A549 cells treated with PBS, coumarin 6-labeled P-LSs, CP20-LSs, and CP50-LSs. **b** Mean fluorescence intensity from (**a**) ($n = 3$, mean ± SD). *$P < 0.05$, **$P < 0.01$, and ***$P < 0.001$. **c** Representative confocal images of A549 cells incubated with coumarin 6-labeled P-LSs, CP20-LSs, and CP50-LSs for 1 h. The nuclei were stained with Hoechst 33342 (blue), and the cell membranes were labeled with Alexa Fluor 555-conjugated WGA (red). Scale bar = 50 μm. **d** Three-dimensional images of A459 cells incubated with coumarin 6-labeled P-LSs, CP20-LSs, and CP50-LSs. Scale bar = 50 μm. **e** Penetration depths of the internalized liposomes in the A549 cells. The fluorescence intensity profiles were obtained in the direction of the white arrows in (**d**). **f** Cell viability of A549 cells after incubation with PTX-loaded liposomes for 48 h ($n = 3$; mean ± SD). **$P < 0.01$, compared with PTX@P-LSs. **g** The IC_{50} values of PTX formulations in (**f**) ($n = 3$; mean ± SD). ***$P < 0.001$ and ****$P < 0.0001$, compared with PTX@CP50-LSs.

that CP50-LSs more effectively accumulated in tumors than P-LSs and CP20-LSs due to the excellent internalization in A549 cells.

Protein adsorption-induced high affinity between liposomes and A549 cells

CP50-LSs with a high amount of CSO modifications showed increased cellular uptake in A549 cells, with high accumulation in A549 tumors. We next investigated the underlying mechanism by analyzing the interaction between liposomes and proteins in the lungs. When entering lung tissues, liposomes first interact with proteins in extracellular spaces, including the interstitial fluid and cell membrane, losing their original surface properties and producing changeable cellular uptake. Hence, we collected extracellular proteins from the lung, incubated them with liposomes for 1 h, and then separated liposome-protein complexes from free proteins. Among the three liposomes, the amount of proteins adsorbed on the P-LS surface was the lowest due to the hydrophilicity of the PEO chains. The protein adsorption of CP50-LSs was 1.5-fold higher than that of CP20-LSs, suggesting that the adsorption of lung extracellular proteins was significantly enhanced by increasing the CSO amount on the liposome surface (Fig. 4a). The adsorbed protein patterns were further visualized using SDS-PAGE. Protein isolates from liposomes showed complex band patterns, indicating that the adsorbed protein layer consists of various proteins spanning a range of densities. Increase in the amount of CSO modification strengthened net lane intensity, consistent with the results of the BCA assay. As shown in Fig. 4b, a similar protein pattern was observed for both CP50-LSs and CP20-LSs, with clear bands of proteins from CP50-LSs and faint bands from CP20-LSs. In addition, the obvious increase in liposome size indicated that the adsorption of lung extracellular proteins may change the properties of liposomes and influence the affinity between liposomes and cells (Fig. 4c).

Collagen is the most abundant protein in lung tissue and is highly expressed in tumors. To investigate the effect of collagen adsorption on the cellular uptake of liposomes, three liposomes

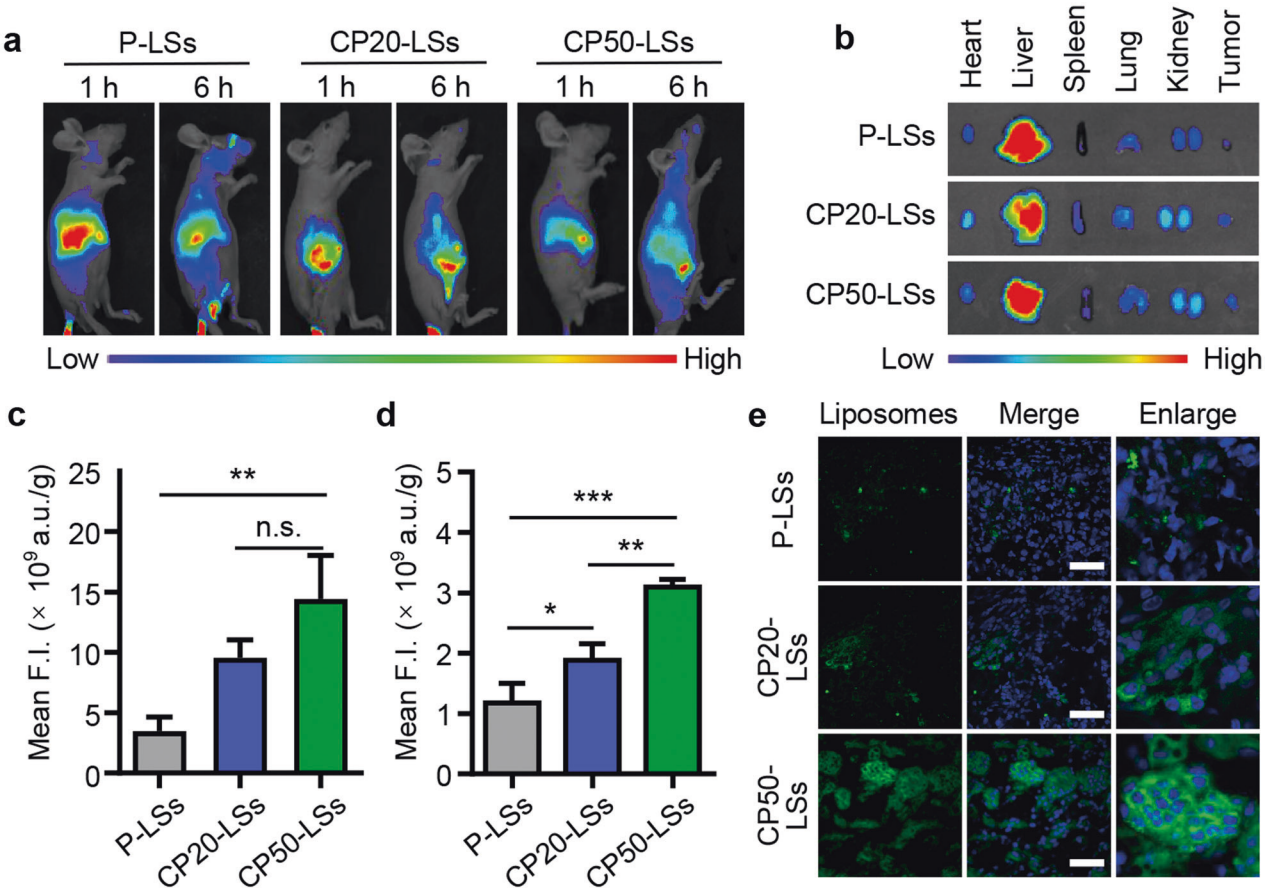

Fig. 3 Tumor accumulation of liposomes in vivo. a Real-time in vivo fluorescence images of mice after intravenous injection of IR783-labeled liposomes. **b** Fluorescence images of organs excised at 6 h postinjection. **c** Biodistribution of IR783-labeled liposomes in lung and (**d**) tumor tissues excised from mice at 6 h postinjection ($n = 3$, mean ± SD). n.s. $P > 0.05$, *$P < 0.05$, **$P < 0.01$, and ***$P < 0.001$. **e** CLSM images of tumor sections showing the distribution of coumarin 6-labeled liposomes (green) in tumor tissues at 24 h postinjection. Scale bar = 50 μm.

were exposed to collagen for 1 h and centrifuged to collect liposome-collagen complexes for analysis. As shown in Fig. 4d, the binding of CP50-LSs with collagen was 3.0 and 1.7 times higher than that of P-LSs and CP20-LSs, respectively. Then, the cellular uptake of liposomes with or without collagen adsorption was determined to explore the effect of collagen on the interaction between liposomes and A549 cells. After preincubation with collagen solutions, the fluorescence intensities of CP50-LSs and CP20-LSs in A549 cells were increased 5.6 and 2.7 times, respectively, indicating that collagen adsorption could enhance the cellular uptake of liposomes. In addition, the signal intensity of CP50-LSs was 6.4- and 3.6-fold higher than that of P-LSs and CP20-LSs, respectively, owing to the high adsorption of collagen caused by the increased CSO amount on the CP50-LS surface (Fig. 4e, f). The collagen adsorbed on the liposome surface may strengthen the affinity between liposomes and tumor cells, resulting in the excellent cellular uptake of CP50-LSs adsorbing massive amounts of collagen. Overall, CP50-LSs could adsorb a large amount of collagen to enhance the interaction between liposomes and tumor cells, promoting cellular uptake in A549 cells and tumor accumulation.

In vivo antitumor efficacy

To explore the potential application of PTX@CP50-LSs in cancer chemotherapy, A549 tumor-bearing nude mice were intravenously injected with free PTX, PTX@P-LSs, PTX@CP20-LSs, PTX@CP50-LSs, or PBS. As shown in Fig. 5a, the average tumor volume in the PBS group increased rapidly, suggesting a high degree of malignancy. Compared with the PBS group, the groups treated with PTX formulations showed inhibited tumor growth to different degrees. Only moderate tumor inhibition was found for the group treated with free PTX, while all the PTX-loaded liposomes showed apparent antitumor effects. PTX@CP50-LSs showed a markedly superior effect with a high tumor inhibition rate of ~90%, significantly slowing tumor growth compared to PTX@P-LSs and PTX@CP20-LSs (Fig. 5a, b). In addition, histological examination of the tumor tissues confirmed the successful destruction of tumor cells by PTX@CP50-LSs, with severe apoptosis across a large area (Fig. 5c). Importantly, negligible changes in body weight were observed during the treatment (Fig. 5d), suggesting that the PTX@CP50-LSs had low systemic toxicity at the applied PTX dosage. These findings suggested that PTX@CP50-LSs exhibited the strongest therapeutic efficacy among the tested liposomes and low toxicity.

DISCUSSION

Liposomes with different CSO modifications engineered in this study were used to enhance the affinity with tumor cells on the basis of stealth liposomes to achieve high accumulation of liposomes in tumor tissues. Pluronic P123, which is similar to PEG chains, could sterically preclude nanoparticles from interacting to reduce nanoparticle aggregation and shield nanoparticles from phagocytosis via the reticuloendothelial system to prolong blood circulation [33]. However, PEG modification could reduce the cellular internalization of nanoparticles because the steric

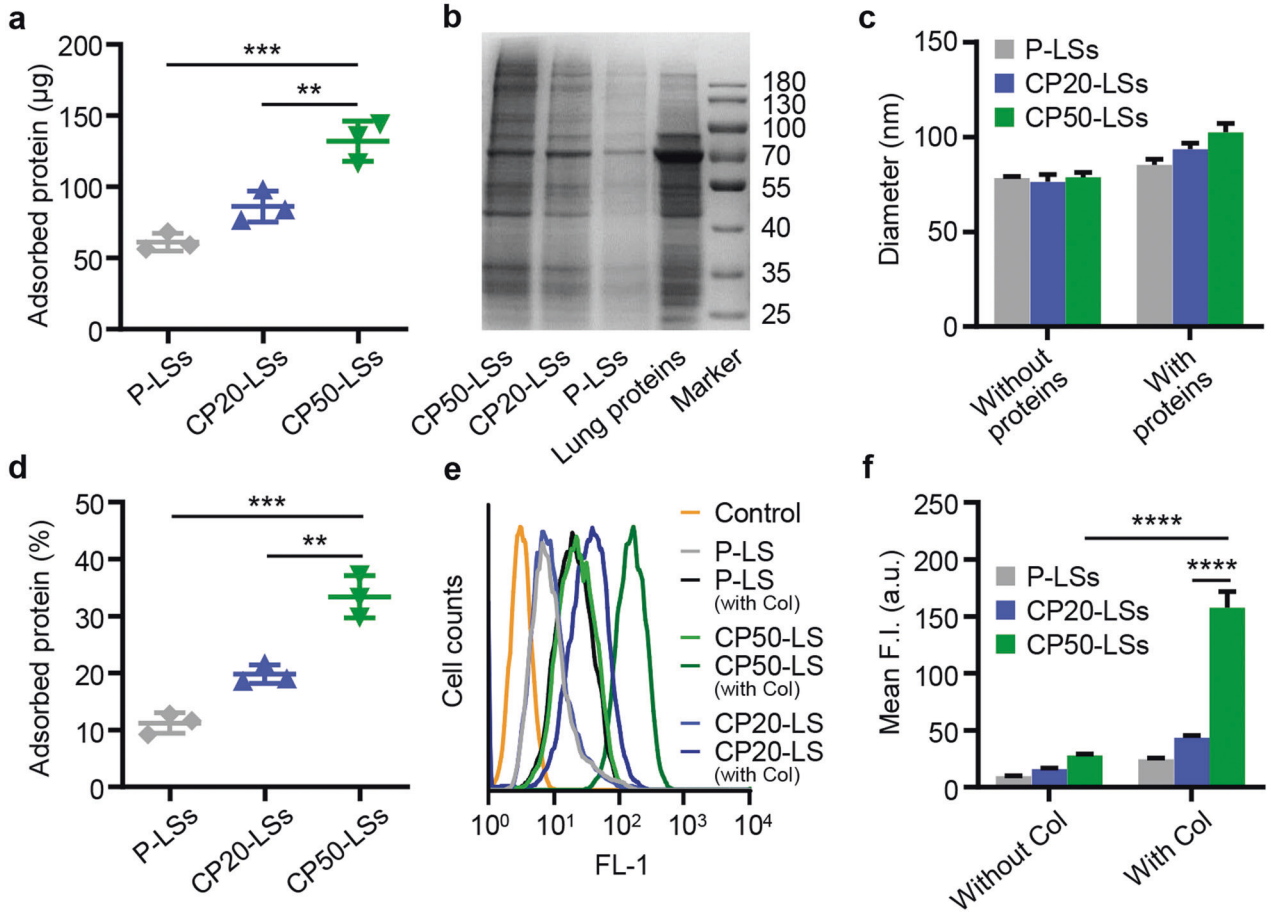

Fig. 4 Protein adsorption induced high affinity between CP50-LSs and A549 cells. a Quantification of proteins adsorbed on the liposome surface ($n = 3$, mean ± SD). $^{**}P < 0.01$ and $^{***}P < 0.001$. **b** Qualitative molecular composition of the adsorbed protein layer on liposomes by SDS-PAGE. **c** The changes in the size of liposomes after incubation with extracellular proteins from the lung ($n = 3$, mean ± SD). **d** Quantification of type I collagen adsorbed on the liposomes ($n = 3$, mean ± SD). $^{**}P < 0.01$ and $^{***}P < 0.001$. **e** Representative flow cytometry histograms and (**f**) fluorescence intensity of P-LSs, CP20-LSs, and CP50-LSs within A549 cells with or without the preadsorption of collagen on the liposome surface ($n = 3$, mean ± SD). $^{****}P < 0.0001$, compared to CP50-LSs preincubated with collagen.

hindrance of PEG chains hinders the interaction between nanoparticles and cells, limiting the drug delivery of PEGylated nanoparticles [34, 35]. In this study, CP50-LSs with a large amount of CSO on the liposome surface exhibited enhanced cellular uptake and uniform distribution in A549 cells, although the PEO chains contained in the liposomes hindered cellular uptake. On the one hand, this may be attributed to the fact that the positive amino groups in the CSO grafted on the terminal hydroxyl of the PEO chain strongly interact with the negatively charged sites on the A549 cell membrane, facilitating the adsorption of CSO-modified liposomes on the cell surface and improving internalization and penetration into the cells. On the other hand, collagen, which is highly expressed in A549 tumors and notably adsorbed on the liposome surface, increased the affinity between liposomes and cells, thereby enhancing the cellular uptake of CP50-LSs. After increased endocytosis, CP50-LSs released PTX rapidly in the endosomal acid environment, increasing the intracellular drug concentration and antitumor effect. The designed CP50-LSs could efficiently deliver PTX to tumor cells due to the improved cellular internalization and rapid intracellular drug release.

When nanoparticles are exposed to the human body, they inevitably interact with bodily fluids and thereby adsorb hundreds of biomolecules. A "biomolecular corona" forms on the surface of nanomaterials and confers new biological identification for nanoparticles, which determines their cellular uptake, immune response, biodistribution, clearance, and toxicity [36, 37]. The protein coronas contain various proteins with different physiological effects. For example, immunoglobulin adsorbed on the nanoparticle surface may promote macrophages to capture nanoparticles [38]. The adsorption of several apolipoproteins can reduce nonspecific cellular uptake in vivo [39]. Transferrin could even be used as a target agent for tumor cell targeting after adsorption on the nanoparticle surface [40]. Therefore, the protein corona, with a controllable composition, may improve the delivery efficiency of nanoparticles in target tissues. In our study, CSO-modified liposomes adsorbed a large amount of proteins with different molecular weights. Among these proteins, collagen is one of the most abundant proteins in the lungs and A549 tumors. The binding of collagen on the CSO-modified liposome surface enhanced the affinity with A549 cells, playing an important role in cellular uptake and tumor accumulation.

In vivo biodistribution studies showed that CP50-LSs exhibited more accumulation in normal lung tissues and A549 subcutaneous tumors than P-LSs, which may be attributed to the bioadhesion of the CSO grafted on the liposome surface and the adsorption of extracellular proteins in the lung. The high accumulation of CP50-LSs in lung tissues may provide an enhanced chance of liposomes entering orthotopic lung tumors. This indicated that the excellent antitumor efficacy of PTX@CP50-LSs proved in the A549 subcutaneous tumor models may occur in the orthotopic xenograft models.

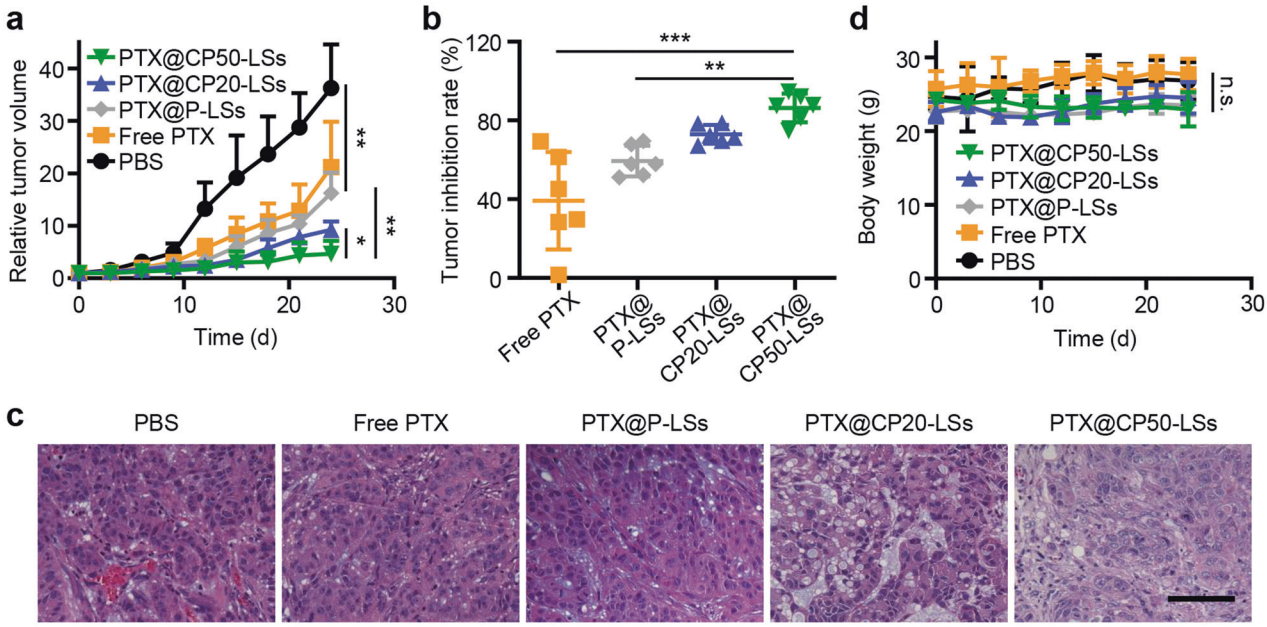

Fig. 5 In vivo antitumor activity after treatment with PTX formulations. a Tumor volume (V/V_0) curves of mice during treatment with different PTX formulations ($n = 6$; mean ± SD). $^*P < 0.05$ and $^{**}P < 0.01$. **b** The tumor inhibition rate of PTX formulations after treatment ($n = 6$; mean ± SD). $^{**}P < 0.01$, $^{***}P < 0.001$. **c** H&E-stained tumor slices on day 22 after treatment with different PTX formulations or PBS. Scale bar = 100 μm. **d** Body weight of tumor-bearing mice over time ($n = 6$; mean ± SD). n.s. $P > 0.05$.

PTX is one of the most effective anticancer drugs and has been widely used in the clinical treatment of nonsmall cell lung cancer. To improve the low water solubility of PTX, Cremophor EL-solubilized PTX called Taxol was first approved by the FDA; however, the serious adverse effects caused by Cremophor EL limit the clinical applications of Taxol [41]. To seek Cremophor EL-free formulations of PTX, albumin-stabilized PTX (Abraxane) and liposomal PTX were developed for the treatment of various cancers. In comparison with Taxol, Abraxane can be administered at a higher dose and shortened infusion time due to the increased intratumor PTX concentration and reduced side effects [42]. Similarly, liposomal PTX showed activities against nonsmall cell lung cancers comparable to Taxol but with lower adverse effects. While most PTX formulations have demonstrated much lower toxicity than Taxol, they show only marginal improvement in treatment efficacy [43]. In this study, we introduced CSO on liposomes to increase the affinity for tumor cells for enhanced tumor accumulation and superior cellular internalization to significantly improve the efficacy of PTX.

In summary, we successfully prepared PTX-loaded liposomes with CSO modification for lung cancer treatment. CSO-modified liposomes decreased the leakage of PTX in the simulated body fluid and promoted PTX release in the simulated endosome/lysosome environment. With increased CSO modifications, CP50-LSs showed enhanced cellular uptake with a wide distribution in A549 cells, leading to the significant inhibition of A549 cell proliferation in vitro compared to P-LSs and CP20-LSs. This may be attributed to the fact that a large amount of collagen that is rich in the tumors adsorbed on the CP50-LSs, enhancing the affinity between liposomes and cells and promoting the internalization of liposomes in A549 cells. In the A549 tumor-bearing mouse model, PTX@CP50-LSs exhibited increased tumor accumulation and improved therapeutic effects with a tumor inhibition rate of ~90% after administration. All these findings suggest that CSO modification may provide a platform for the design of nanoparticle delivery systems for lung cancer treatment.

ACKNOWLEDGEMENTS

This work was supported by the National Natural Science Foundation of China (81973250), the National Science and Technology Major Project (2018ZX09721002-003) and the National Key Research and Development Program of China (NBHY-2017-J1-3).

AUTHOR CONTRIBUTIONS

RW, XXZ, and YG designed the project; YQM and JJZ prepared the liposomes. YQM, MSC, and LMG designed and performed all experiments. All authors analyzed and discussed the data. YQM, MSC, XZ, and XXZ wrote the manuscript.

ADDITIONAL INFORMATION

Competing interests: The authors declare no competing interests.

REFERENCES

1. Wong MCS, Lao XQ, Ho KF, Goggins WB, Tse SLA. Incidence and mortality of lung cancer: global trends and association with socioeconomic status. Sci Rep. 2017;7:14300–8.
2. Zappa C, Mousa SA. Non-small cell lung cancer: current treatment and future advances. Transl Lung Cancer Res. 2016;5:288–300.
3. Zhang Y, Yang J, Ding M, Li L, Lu Z, Zhang Q, et al. Tumor-penetration and antitumor efficacy of cetuximab are enhanced by co-administered iRGD in a murine model of human NSCLC. Oncol Lett. 2016;12:3241–9.
4. Liang XJ, Chen C, Zhao Y, Wang PC. Circumventing tumor resistance to chemotherapy by nanotechnology. Methods Mol Biol. 2010;596:467–88.
5. Decuzzi P, Godin B, Tanaka T, Lee SY, Chiappini C, Liu X, et al. Size and shape effects in the biodistribution of intravascularly injected particles. J Control Release. 2010;141:320–7.
6. Yu T, Hubbard D, Ray A, Ghandehari H. In vivo biodistribution and pharmacokinetics of silica nanoparticles as a function of geometry, porosity and surface characteristics. J Control Release. 2012;163:46–54.
7. Torchilin VP. Multifunctional, stimuli-sensitive nanoparticulate systems for drug delivery. Nat Rev Drug Discov. 2014;13:813–27.
8. Lim YH, Tiemann KM, Hunstad DA, Elsabahy M, Wooley KL. Polymeric nanoparticles in development for treatment of pulmonary infectious diseases. Wiley Interdiscip Rev Nanomed Nanobiotechnol. 2016;8:842–71.
9. Lammers T, Kiessling F, Hennink WE, Storm G. Drug targeting to tumors: principles, pitfalls and (pre-) clinical progress. J Control Release. 2012;161:175–87.

10. Agnoletti M, Rodriguez-Rodriguez C, Klodzinska SN, Esposito TVF, Saatchi K, Morck Nielsen H, et al. Monosized polymeric microspheres designed for passive lung targeting: biodistribution and pharmacokinetics after intravenous administration. ACS Nano. 2020;14:6693–706.
11. Au KM, Min Y, Tian X, Zhang L, Perello V, Caster JM, et al. Improving cancer chemoradiotherapy treatment by dual controlled release of wortmannin and docetaxel in polymeric nanoparticles. ACS Nano. 2015;9:8976–96.
12. Pack DW, Hoffman AS, Pun S, Stayton PS. Design and development of polymers for gene delivery. Nat Rev Drug Discov. 2005;4:581–93.
13. Merkel OM, Beyerle A, Librizzi D, Pfestroff A, Behr TM, Sproat B, et al. Nonviral siRNA delivery to the lung: investigation of PEG-PEI polyplexes and their in vivo performance. Mol Pharmacol. 2009;6:1246–60.
14. Jin H, Xu CX, Kim HW, Chung YS, Shin JY, Chang SH, et al. Urocanic acid-modified chitosan-mediated PTEN delivery via aerosol suppressed lung tumorigenesis in K-ras(LA1) mice. Cancer Gene Ther. 2008;15:275–83.
15. Nascimento AV, Singh A, Bousbaa H, Ferreira D, Sarmento B, Amiji MM. Mad2 checkpoint gene silencing using epidermal growth factor receptor-targeted chitosan nanoparticles in non-small cell lung cancer model. Mol Pharmacol. 2014;11:3515–27.
16. Muzzarelli R, Baldassarre V, Conti F, Ferrara P, Biagini G, Gazzanelli G, et al. Biological activity of chitosan: ultrastructural study. Biomaterials 1988;9:247–52.
17. Muzzarelli RA. Human enzymatic activities related to the therapeutic administration of chitin derivatives. Cell Mol Life Sci. 1997;53:131–40.
18. George M, Abraham TE. Polyionic hydrocolloids for the intestinal delivery of protein drugs: alginate and chitosan-a review. J Control Release. 2006;114:1–14.
19. Sinha VR, Singla AK, Wadhawan S, Kaushik R, Kumria R, Bansal K, et al. Chitosan microspheres as a potential carrier for drugs. Int J Pharm. 2004;274:1–33.
20. Mohammed MA, Syeda JTM, Wasan KM, Wasan EK. An overview of chitosan nanoparticles and its application in non-parenteral drug delivery. Pharmaceutics 2017;9:53–78.
21. Pavinatto FJ, Pavinatto A, Caseli L, dos Santos DS, Nobre TM, Zaniquelli MED, et al. Interaction of chitosan with cell membrane models at the air-water interface. Biomacromolecules 2007;8:1633–40.
22. Huang M, Ma Z, Khor E, Lim LY. Uptake of FITC-chitosan nanoparticles by A549 cells. Pharm Res. 2002;19:1488–94.
23. Vijayakurup V, Thulasidasan AT, Shankar GM, Retnakumari AP, Nandan CD, Somaraj J, et al. Chitosan encapsulation enhances the bioavailability and tissue retention of curcumin and improves its efficacy in preventing B[a]P-induced lung carcinogenesis. Cancer Prev Res (Philos). 2019;12:225–36.
24. Jia LJ, Li ZY, Zhang DR, Zhang Q, Shen JY, Guo HJ, et al. Redox-responsive catiomer based on PEG-ss-chitosan oligosaccharide-ss-polyethylenimine copolymer for effective gene delivery. Polym Chem-UK. 2013;4:156–65.
25. Pillai CKS, Paul W, Sharma CP. Chitin and chitosan polymers: chemistry, solubility and fiber formation. Prog Polym Sci. 2009;34:641–78.
26. Muanprasat C, Chatsudthipong V. Chitosan oligosaccharide: biological activities and potential therapeutic applications. Pharmacol Ther. 2017;170:80–97.
27. Abrica-Gonzalez P, Zamora-Justo JA, Sotelo-Lopez A, Vazquez-Martinez GR, Balderas-Lopez JA, Munoz-Diosdado A, et al. Gold nanoparticles with chitosan, N-acylated chitosan, and chitosan oligosaccharide as DNA carriers. Nanoscale Res Lett. 2019;14:258–71.
28. Hu FQ, Chen WW, Zhao MD, Yuan H, Du YZ. Effective antitumor gene therapy delivered by polyethylenimine-conjugated stearic acid-g-chitosan oligosaccharide micelles. Gene Ther. 2013;20:597–606.
29. Bareschino MA, Schettino C, Rossi A, Maione P, Sacco PC, Zeppa R, et al. Treatment of advanced non small cell lung cancer. J Thorac Dis. 2011;3:122–33.
30. Ohashi T, Yoshimasu T, Oura S, Kokawa Y, Kawago M, Hirai Y, et al. Class III beta-tubulin expression in non-small cell lung cancer: a predictive factor for paclitaxel response. Anticancer Res. 2015;35:2669–74.
31. Sun W, Jiang Y, He F. Extraction and proteome analysis of liver tissue interstitial fluid. Methods Mol Biol. 2011;728:247–57.
32. De Jaeghere F, Allemann E, Feijen J, Kissel T, Doelker E, Gurny R. Cellular uptake of PEO surface-modified nanoparticles: Evaluation of nanoparticles made of PLA: PEO diblock and triblock copolymers. J Drug Target. 2000;8:143–53.
33. Suk JS, Xu QG, Kim N, Hanes J, Ensign LM. PEGylation as a strategy for improving nanoparticle-based drug and gene delivery. Adv Drug Deliv Rev. 2016;99:28–51.
34. Zhu YQ, Chen C, Cao ZY, Shen S, Li LS, Li DD, et al. On-demand PEGylation and dePEGylation of PLA-based nanocarriers via amphiphilic mPEG-TK-Ce6 for nanoenabled cancer chemotherapy. Theranostics 2019;9:8312–20.
35. Soenen SJ, Manshian BB, Abdelmonem AM, Montenegro JM, Tan S, Balcaen L, et al. The cellular interactions of PEGylated gold nanoparticles: effect of PEGylation on cellular uptake and cytotoxicity. Part Part Syst Char. 2014; 31:794–800.
36. Aggarwal P, Hall JB, McLeland CB, Dobrovolskaia MA, McNeil SE. Nanoparticle interaction with plasma proteins as it relates to particle biodistribution, biocompatibility and therapeutic efficacy. Adv Drug Deliv Rev. 2009;61:428–37.
37. Monopoli MP, Aberg C, Salvati A, Dawson KA. Biomolecular coronas provide the biological identity of nanosized materials. Nat Nanotechnol. 2012;7: 779–86.
38. Jenney CR, Anderson JM. Adsorbed serum proteins responsible for surface dependent human macrophage behavior. J Biomed Mater Res. 2000;49:435–47.
39. Schottler S, Becker G, Winzen S, Steinbach T, Mohr K, Landfester K, et al. Protein adsorption is required for stealth effect of poly(ethylene glycol)- and poly (phosphoester)-coated nanocarriers. Nat Nanotechnol. 2016;11:372–7.
40. Wang XY, Wang MZ, Lei R, Zhu SF, Zhao YL, Chen CY. Chiral surface of nanoparticles determines the orientation of adsorbed transferrin and its interaction with receptors. ACS Nano. 2017;11:4606–16.
41. Marupudi NI, Han JE, Li KW, Renard VM, Tyler BM, Brem H. Paclitaxel: a review of adverse toxicities and novel delivery strategies. Expert Opin Drug Saf. 2007;6: 609–21.
42. Green MR, Manikhas GM, Orlov S, Afanasyev B, Makhson AM, Bhar P, et al. Abraxane, a novel Cremophor-free, albumin-bound particle form of paclitaxel for the treatment of advanced non-small-cell lung cancer. Ann Oncol. 2006;17: 1263–8.
43. Wang F, Porter M, Konstantopoulos A, Zhang P, Cui H. Preclinical development of drug delivery systems for paclitaxel-based cancer chemotherapy. J Control Release. 2017;267:100–18.